Separation Science and Technology
Publication details, including instructions for authors and subscription information:
http://www.informaworld.com/smpp/title~content=t713708471

A COMPARISON OF OPTIMAL INTERNALLY STAGED PERMEATOR AND EXTERNAL TWO-STAGE MODULE DESIGNS FOR O_2 ENRICHMENT FROM AIR

B. Liu[a]; G. G. Lipscomb[a]; J. A. Jensvold[b]
[a] University of Toledo, Toledo, OH, U.S.A. [b] MG Generon, Pittsburg, CA, U.S.A.

Online publication date: 31 August 2001

To cite this Article Liu, B. , Lipscomb, G. G. and Jensvold, J. A.(2001) 'A COMPARISON OF OPTIMAL INTERNALLY STAGED PERMEATOR AND EXTERNAL TWO-STAGE MODULE DESIGNS FOR O_2 ENRICHMENT FROM AIR', Separation Science and Technology, 36: 11, 2385 — 2409
To link to this Article: DOI: 10.1081/SS-100106099
URL: http://dx.doi.org/10.1081/SS-100106099

SEPARATION SCIENCE AND TECHNOLOGY, 36(11), 2385–2409 (2001)

A COMPARISON OF OPTIMAL INTERNALLY STAGED PERMEATOR AND EXTERNAL TWO-STAGE MODULE DESIGNS FOR O_2 ENRICHMENT FROM AIR

B. Liu,[1] G.G. Lipscomb,[1,*] and J. A. Jensvold[2]

[1]Chemical and Environmental Engineering, University of Toledo, Toledo, OH 43606, USA
[2]MG Generon, Pittsburg, CA 94565, USA

ABSTRACT

We present a performance comparison of internally staged permeator (ISP) and external two-stage module designs for oxygen enrichment from air. Design and operational parameters were selected to maximize product recovery. Theoretically, the optimized external two-stage design performs almost as well as the optimal ISP design; the optimal ISP configuration (co-counter design) gives slightly higher product recovery but requires more membrane area than the optimal external two-stage design. Experimental performance measurements of the external two-stage design are in good agreement with theoretical predictions.

*Corresponding author. Fax: (419) 530-8086; E-mail: glenn.lipscomb@utoledo.edu

INTRODUCTION

Although membrane-based gas separation processes are now widely used in industry, their ability to successfully compete with existing separation processes will rely on improved performance, especially at higher product purities. The literature is replete with studies of new membrane materials that potentially offer better performance. However, the development of improved module designs has received less attention.

Conventional module designs commonly utilize one of three flow configurations: permeate and retentate flowing in cocurrent, countercurrent, or cross-flow directions. The performances of these designs have been studied extensively (1). The countercurrent design offers the best performance in the absence of boundary-layer mass transfer resistances and significant lumen pressure drop.

Attempts to improve module performance have relied primarily on sending a portion of the product streams back to the feed or to another module. Permeate recycle schemes (2,3) are examples of the former while staged module designs (4–6), including the continuous membrane column (7,8), are examples of the latter.

The internally staged permeator (ISP) is one of the most interesting developments in module design. As originally proposed by Sidhoum et al. (9), the ISP consists of two sets of fibers that are uniformly mixed within the bundle. In operation, the high-pressure feed to one set of fibers (the first stage) produces a permeate at an intermediate pressure. This permeate simultaneously flows around the second fiber group (the second stage) to produce a lower-pressure permeate. The concentration of the faster permeating species in the low-pressure permeate can be greatly enriched over that achievable in a conventional design without additional energy consumption by the system. This enrichment comes at the cost of lower membrane productivity.

ISP performance, as measured by permeate recovery, is sensitive to the value of the intermediate pressure and the area ratio between the two sets of fibers. Proper selection of these parameters maximizes permeate recovery.

The performance of ISP designs has been extensively investigated (10–16). This body of work demonstrates that optimized ISP designs can offer higher permeate recovery, at a fixed purity, than does a single-stage design. Moreover, the highest permeate purity that can be produced exceeds that achievable in a single stage. Of the nine designs proposed in the literature (16), the co-counter design, in which the high-pressure retentate and intermediate-pressure permeate flow cocurrently while the intermediate-pressure permeate and low-pressure permeate flow countercurrently, provides the highest recovery but requires the greatest membrane area.

As an alternative to ISP designs, one can place 2 single stages in series with the permeate from the first stage used as the feed to the second stage. The second

stage produces the low-pressure permeate. As in the ISP design, the intermediate-pressure permeate is maintained at a pressure between that of the feed and low-pressure permeate. In comparison to ISP designs, the external two-stage design requires additional plumbing and module housings. However, one would expect the cost of manufacture to be lower due to decreased module complexity.

Although the literature recognizes that the external two-stage design is a competitor with ISP designs (10,14), it is unclear which model offers superior performance. Sidhoum, Majumdar, and Sirkar (10) indicate that the ISP designs are superior to an external two-stage module design while Li and Hughes (14) conclude that the external two-stage design is superior to some ISP designs but inferior to others. It is also unclear to what extent both sets of authors tried to optimize the designs they considered.

We present here an optimization study of the external two-stage and ISP module designs. Theoretically, design and operational parameters for both designs were selected to maximize permeate recovery for the production of oxygen from air. Performance predictions for the optimized designs indicate that the ISP would yield only slightly higher permeate recovery but would require more membrane area. Experimental measurements for an external two-stage design are in good agreement with theoretical predictions and confirm that the external two-stage design can perform nearly as well as the ISP design.

THEORETICAL

We considered 3 membrane designs: 1) a single countercurrent stage, 2) two countercurrent stages in series, and 3) a co-counter ISP. The co-counter ISP design yields the highest permeate recovery, for a specific permeate purity, of all ISP designs (16). Therefore, its performance represents the best achievable with an ISP design. This system is compared to a comparable external two-stage system consisting of two countercurrent stages in series; the permeate from the first stage is kept at an intermediate-pressure and is fed to a second stage that produces the low-pressure permeate product. Experimental and theoretical evaluation of the performance of this external two-stage system, relative to the ISP design, is the objective of this study. The single countercurrent stage is included to provide a performance baseline.

The performance equations for each design are based on the following assumptions:

1. binary gas mixtures;
2. constant membrane transport properties: The permeance of each gas component is equal to that of the pure gas and is independent of pressure;
3. negligible gas-phase concentration polarization;

MARCEL DEKKER, INC.
270 Madison Avenue, New York, New York 10016

4. axial diffusion negligible relative to convective transport;
5. pressure drops in the lumen and shell have a negligible effect on performance predictions; and
6. isothermal operation.

Previous work (16) demonstrates that inclusion of lumen pressure drops has a negligible effect on ISP performance predictions for i.d. measurements as small as 100 μm. We could not determine fiber i.d. values for the single-stage modules used experimentally without destroying the modules, but this value is significantly smaller than the reported o.d. of 450 μm. See Table 1 for a list of module properties for the two-stage system.

The detailed development of the performance equations and procedures for their solutions are available in the literature (16).

Co-counter ISP

As illustrated in Fig. 1, in the co-counter ISP design, the high-pressure retentate flows cocurrently with the intermediate-pressure permeate while the intermediate-pressure permeate flows countercurrently to the low-pressure permeate. For this system, the performance equations are (16)

$$\frac{d(x\theta_H)}{dZ} = -J_{HI}^A \tag{1}$$

$$\frac{d(\theta_H)}{dZ} = -J_{HI}^A - J_{HI}^B \tag{2}$$

$$\frac{d(y_I\theta_I)}{dZ} = J_{HI}^A - J_{IL}^A \tag{3}$$

$$\frac{d(\theta_I)}{dZ} = J_{HI}^A + J_{HI}^B - J_{IL}^A - J_{IL}^B \tag{4}$$

Table 1. Module Properties of Two-Stage System

Model	PPA-22AD
Membrane	Polysulfone hollow fiber
Fiber o.d.	450 micron nominal
Active fiber length	53 cm
Membrane area	$A_1 = A_2 = 2.23 \times 10^4$ cm^2
Packing density	47 %
Maximum operating pressure	100 psig
Permeance 10^5 [cm^3(STP)/cm^{2}s cm Hg] $\cdot$ 10^5	O_2: 2.407
	N_2: 0.414

Marcel Dekker, Inc.
270 Madison Avenue, New York, New York 10016

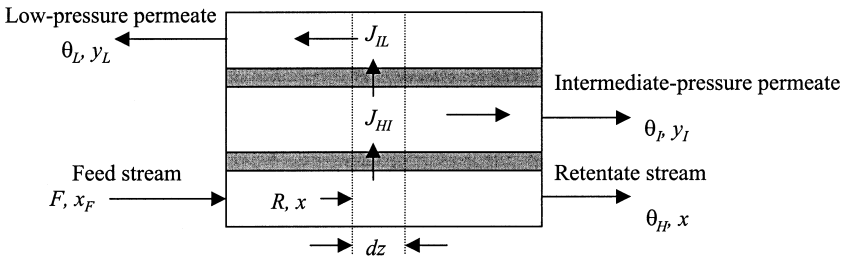

Figure 1. Internally staged permeator: co-counter flow pattern.

$$\frac{d(y_L\theta_L)}{dZ} = -J_{IL}^A \tag{5}$$

$$\frac{d(\theta_L)}{dZ} = -J_{IL}^A - J_{IL}^B \tag{6}$$

where the dimensionless fast-gas (i.e., more permeable component) permeation rate from the high-pressure retentate to the intermediate-pressure permeate, J_{HI}^A, is given by

$$J_{HI}^A = \alpha\, N^h\, (x - \gamma_{IH}\, y_I) \tag{7}$$

where the superscript A denotes the fast gas; α is the permselectivity; x is the fast gas mole fraction in the retentate; y_I is the fast gas mole fraction in the intermediate-pressure permeate; and γ_{IH} is the ratio of the intermediate permeate to retentate pressure, the subscript H refers to the high-pressure retentate, and the subscript I refers to the intermediate-pressure permeate. N^h is a dimensionless mass-transfer coefficient or membrane area defined as

$$N^h = \frac{A_{HI}(P/L)P_H}{F} \tag{8}$$

where A_{HI} is the total area available for permeation from the retentate to the intermediate-pressure permeate; P is the intrinsic slow gas permeability for the membrane; l is the effective membrane thickness; p_H is the retentate pressure; and F is the total feed rate. One may also view N^h as a dimensionless inverse flow rate: Increased values of N^h correspond to decreased flow rates. The dimensionless slow-gas permeation rate, J_{HI}^B, is given by

$$J_{HI}^B = N^h[(1 - x) - \gamma_{IH}\,(1 - y_I)] \tag{9}$$

where the superscript B denotes the slow gas. The dimensionless fast-gas permeation rate from the intermediate-pressure permeate to the low-pressure permeate is given by

$$J_{IL}^A = \alpha N^h \gamma_{IH} Ar(y_I - \gamma_{LI}\, y_L) \tag{10}$$

MARCEL DEKKER, INC.
270 Madison Avenue, New York, New York 10016

where Ar is a ratio of the area available for intermediate- to low-pressure permeation to the area available for high- to intermediate-pressure permeation; γ_{LI} is the ratio of low- to intermediate-permeate pressure; and y_L is the fast-gas mole fraction in the low-pressure permeate. The slow-gas permeation rate is given by

$$J^B_{IL} = N^h \gamma_{IH} Ar[(1 - y_I) - \gamma_{LI}(1 - y_L)] \tag{11}$$

The boundary conditions for the co-counter flow pattern are given by the following:

$$Z = 0, \quad \theta_H = 1, \quad x = x_F,$$

$$\theta_I = 0, \quad \text{and} \quad y_I = \frac{J^A_{HI} - J^A_{IL}}{(J^A_{HI} - J^A_{IL}) + (J^B_{HI} - J^B_{IL})} \tag{12}$$

$$Z = 1, \quad \theta_L = 0, \quad \text{and} \quad y_L = \frac{J^A_{IL}}{J^A_{IL} + J^B_{IL}} \tag{13}$$

External Two-Stage System

The external two-stage module design is illustrated in Fig. 2. Mass balances on each stage yield the following performance equations.

First Stage:

$$\frac{d(x\theta_H)}{dZ} = -J^A_{HI1} \tag{14}$$

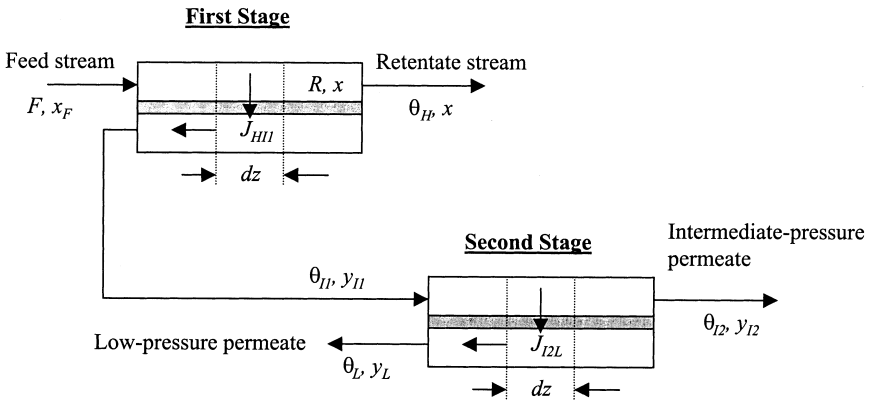

Figure 2. External two-stage design.

MARCEL DEKKER, INC.
270 Madison Avenue, New York, New York 10016

$$\frac{d(\theta_H)}{dZ} = -J^A_{HI1} - J^B_{HI1} \tag{15}$$

$$\frac{d(y_{I1}\theta_{I1})}{dZ} = \frac{d(x\theta_H)}{dZ} \tag{16}$$

$$\frac{d(\theta_{I1})}{dZ} = \frac{d(\theta_H)}{dZ} \tag{17}$$

where

$$J^A_{HI1} = \alpha N^h (x - \gamma_{I1H}\, y_{I1}) \tag{18}$$

$$J^B_{HI1} = N^h[(1 - x) - \gamma_{I1H}\,(1 - y_{I1})] \tag{19}$$

The variable definitions for the external two-stage design are the same as those for the ISP design. The subscripts 1 and 2 represent the first and second stage, respectively.

Boundary conditions for the first stage are

$$Z = 0, \quad \theta_H = 1, \quad \text{and} \quad x = x_F \tag{20}$$

$$Z = 1, \quad \theta_{I1} = 0, \quad \text{and} \quad y_{I1} = \frac{J^A_{HI1}}{J^A_{HI1} + J^B_{HI1}} \tag{21}$$

Second Stage:

$$\frac{d(y_{I2}\theta_{I2})}{dZ} = -J^A_{I2L} \tag{22}$$

$$\frac{d(\theta_{I2})}{dZ} = -J^A_{I2L} - J^B_{I2L} \tag{23}$$

$$\frac{d(y_L\theta_L)}{dZ} = \frac{d(y_{I2}\theta_{I2})}{dZ} \tag{24}$$

$$\frac{d(\theta_L)}{dZ} = \frac{d(\theta_{I2})}{dZ} \tag{25}$$

where

$$J^A_{I2L} = \alpha N^h \gamma_{I1H} Ar(y_{I2} - \gamma_{LI2} y_L) \tag{26}$$

$$J^B_{I2L} = N^h \gamma_{I1H} Ar[(1 - y_{I2}) - \gamma_{LI2}\,(1 - y_L)] \tag{27}$$

Boundary conditions for the second stage are

$$Z = 0, \quad \theta_{I2} = \theta_{I1}\,|_{\,Z=0} \quad \text{and} \quad y_{I2} = y_{I1}\,|_{\,Z=0} \tag{28}$$

$$Z = 1, \quad \theta_L = 0, \quad \text{and} \quad y_L = \frac{J^A_{I2L}}{J^A_{I2L} + J^B_{I2L}} \tag{29}$$

where $\theta_{I1}\big|_{Z=0}$ is the value of θ_{I1} at $Z = 0$ for the first stage.

The performance equations for the ISP design are split boundary value problems. We used the finite difference method to obtain a numerical approximation to their solutions. Derivatives were approximated by second-order differences except at $Z = 0$ and $Z = 1$ where a first-order difference was used. This solution algorithm converges more rapidly than the more commonly used numerical integration with shooting method.

For the external two-stage design, the performance equations for the first stage were solved first and then the equations for the second were solved. Numerical integration with shooting and finite difference approximations are equally effective for solving the performance equations.

Both the ISP and external two-stage designs require specification of three operational variables:

1. Pressure ratio. $\gamma_{IH} = p_I/p_H$, the ratio of the intermediate to high pressure, or $\gamma_{LI} = p_L/p_I$, the ratio of the low to the intermediate pressure.
2. Area ratio. Ar, the ratio of the area available for intermediate- to low-pressure permeation to that available for high- to intermediate-pressure permeation.
3. Dimensionless mass-transfer coefficient or membrane area, N^h. The total dimensionless area for the external two-stage and ISP designs is given by $N^h(1+Ar)$, while the dimensionless area for the single stage is equal to N^h.

Performance is highly sensitive to these variables. Here we selected values for γ_{IH}, Ar, and N^h to maximize low-pressure permeate recovery (i.e., θ_L at the low-pressure permeate outlet). The Nelder-Mead simplex search algorithm, implemented in MATLAB (17) as the function FMINS, was used to perform the optimization. This algorithm was started from an initial guess for Ar and γ_{IH} to find values that maximize θ_L (or minimize $1/\theta_L$) at a specified low-pressure permeate composition; the value of N^h was adjusted to produce the specified composition for each Ar and γ_{IH} . Unfortunately, one cannot guarantee that the algorithm will return values that correspond to a global minimum. The value may correspond to a local minimum instead. To evaluate if a local minimum was found, the search algorithm was started from a range of initial guesses and some optimizations were performed by systematically searching the feasible parameter space for Ar and γ_{IH} . In all cases, no other minima were found.

EXPERIMENTAL

Because extensive experimental comparisons are given in the literature for the ISP designs, we report performance results only for the external two-stage sys-

MARCEL DEKKER, INC.
270 Madison Avenue, New York, New York 10016

tem. The system we used consisted of 2 hollow fiber membrane permeators (Permea Inc., St. Louis, MO, Model PPA-22AD) containing polysulfone hollow fiber membranes. The module properties are listed in Table 1 and the experimental apparatus is illustrated in Fig. 3.

In experiments, compressed air was introduced to the lumen side of the first-stage module. The feed line consisted of two filters in series to remove entrained liquids and particulates. Then the pressure of the feed was set and regulated. The high-pressure retentate stream, enriched in nitrogen, passed through a digital mass flow meter (Sierra Instruments Inc., Model 820), a digital oxygen analyzer (Engineering Systems and Designs, Model 600 Oxan), and then was vented to the atmosphere. The retentate flow rate was controlled by a needle valve.

The oxygen enriched permeate stream from the first stage was introduced to the lumen side of the second-stage module to produce a low-pressure permeate stream. The retentate stream from the second stage (i.e., the intermediate-pressure permeate) passed through a digital mass flow meter and a digital oxygen analyzer. The pressure of the intermediate-pressure permeate stream was controlled by a needle valve in the retentate line of the second stage. The low-pressure permeate, further enriched in oxygen, was withdrawn countercurrently from the shell of the second-stage module and passed through a digital flow meter and an oxygen analyzer.

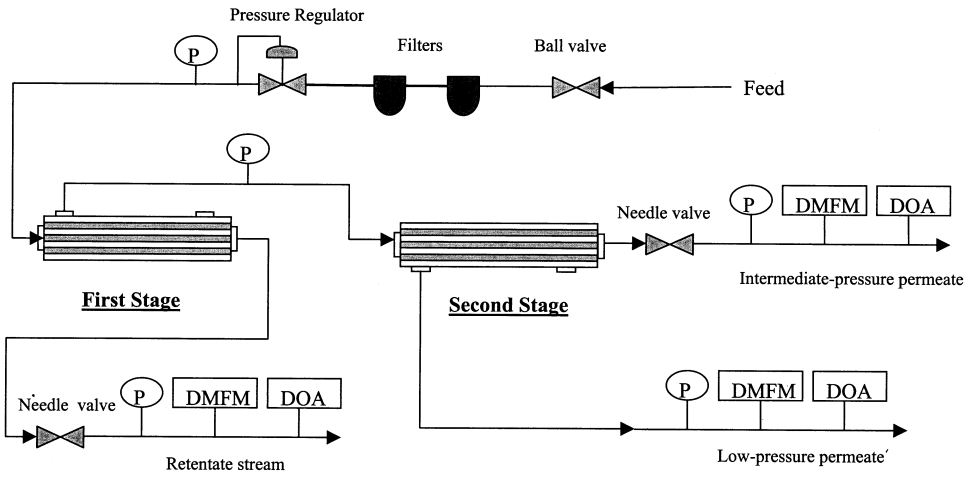

Figure 3. Experimental apparatus for external two-stage design.

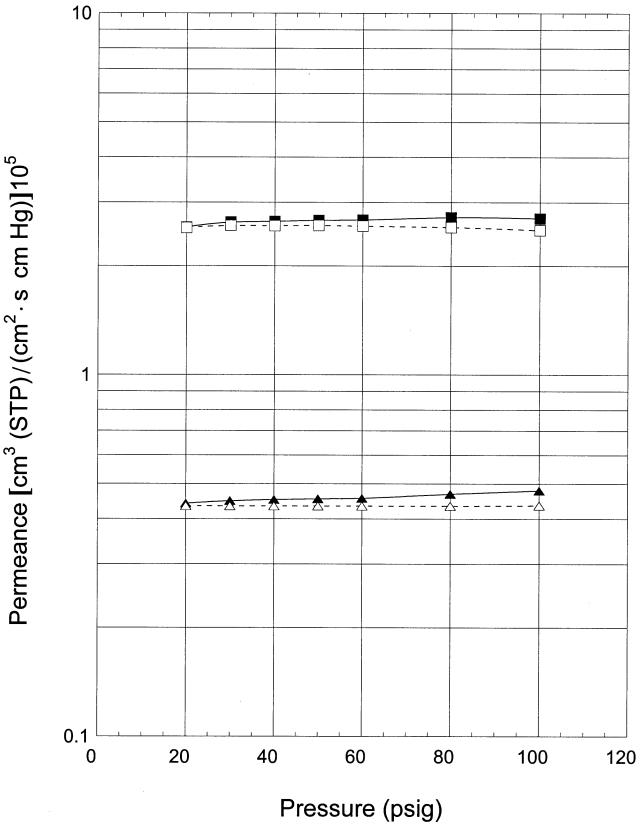

Figure 4. Pure component permeances for the first stage: ▲ Nitrogen (lumen feed); ■ Oxygen (lumen feed); △ Nitrogen (shell feed); □ Oxygen (shell feed).

Pure component permeation experiments were conducted to determine oxygen and nitrogen permeances for each stage. Permeances were calculated from the permeate flow rates for various permeation pressure differences. The retentate line was closed for both lumen and shell feed measurements.

To maximize permeate recovery at a fixed permeate composition, the flow rate of the intermediate-pressure permeate was adjusted to change the pressure of the stream. The specific permeate composition was achieved by varying the feed flow rate. Flow rate, composition, and pressure of all streams were measured at steady state. Mass balances were within 5% for all experiments. In addition, measured pressure drops for the lumen and shell were less than 1 psi.

MARCEL DEKKER, INC.
270 Madison Avenue, New York, New York 10016

RESULTS

Individual Module Permeance

The measured permeances for oxygen and nitrogen as functions of pressure difference are shown in Figs. 4 and 5. The shell feed permeances are essentially constant for both modules over the pressure range tested. The lumen feed permeances were slightly higher than the shell feed permeances. In addition, the lumen feed permeances increased slightly with pressure. This change may have been due to a slight increase in fiber size with increasing pressure (18). However, the increase over the measured pressure range was small and we did not pursue an explanation of the increase.

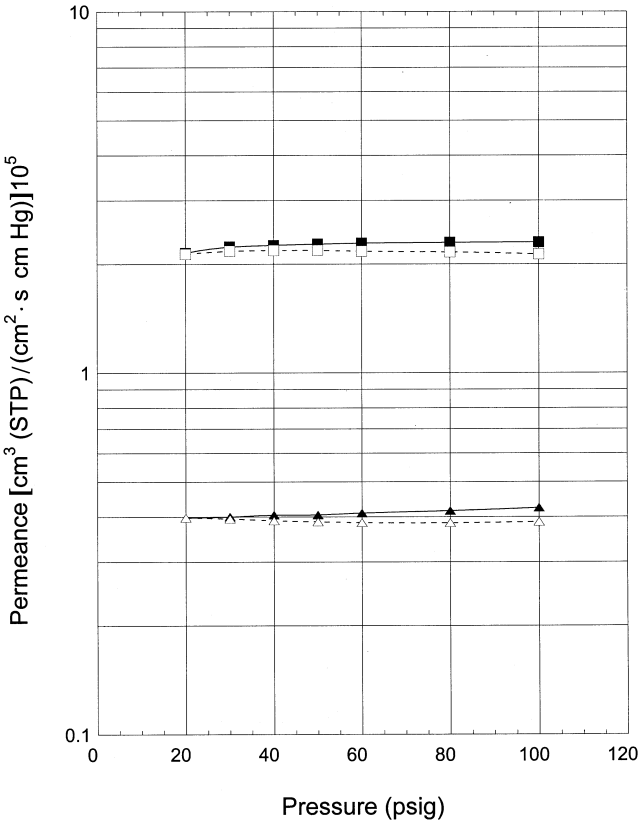

Figure 5. Pure component permeances for the second stage: ▲ Nitrogen (lumen feed); ■ Oxygen (lumen feed); △ Nitrogen (shell feed); □ Oxygen (shell feed).

MARCEL DEKKER, INC.
270 Madison Avenue, New York, New York 10016

The lack of a strong pressure dependence suggests that the excess free volume contribution to permeability is small. As a result, one would expect only small changes in permeance for mixed gas permeation as observed previously for oxygen and nitrogen (18). The measured values are given in Table 1.

Individual Module Performance

The measured performance for oxygen enrichment from air for each stage is shown in Fig. 6. Operating conditions for the experiments and simulations are listed in Table 2. The feed flow rate was varied to obtain results for different permeate purities. Figure 6 indicates that the experimental results are in agreement with theoretical predictions for each single stage.

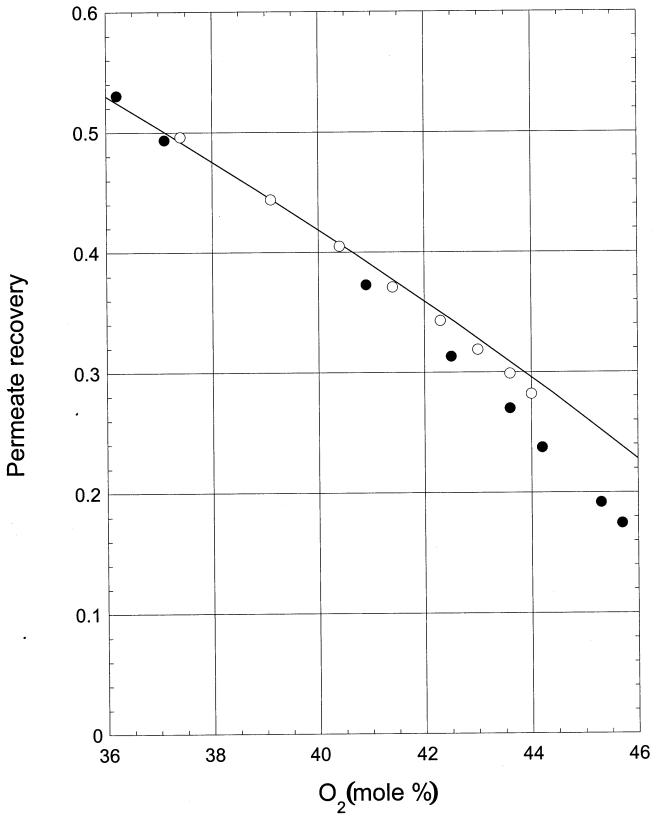

Figure 6. Comparison between experimental measurements and theoretical predictions of stage performance: — Theory (single stage); ○ Experiment (first stage); ● Experiment (second stage). Note that the theoretical predictions for the two stages overlap.

MARCEL DEKKER, INC.
270 Madison Avenue, New York, New York 10016

Table 2. Operating Conditions for Experiments and Simulations of O_2 Enrichment from Air

Feed pressure (psig)	85
Low-pressure permeate	atmospheric
Feed composition (mole fraction)	O_2: 20.9
	N_2: 79.1

Stage Optimization

Theoretical optimization results for the external two-stage and ISP designs are shown in Fig. 7, where the maximum permeate recovery for each system is given as a function of oxygen purity. Figure 7 also contains the results for a sin-

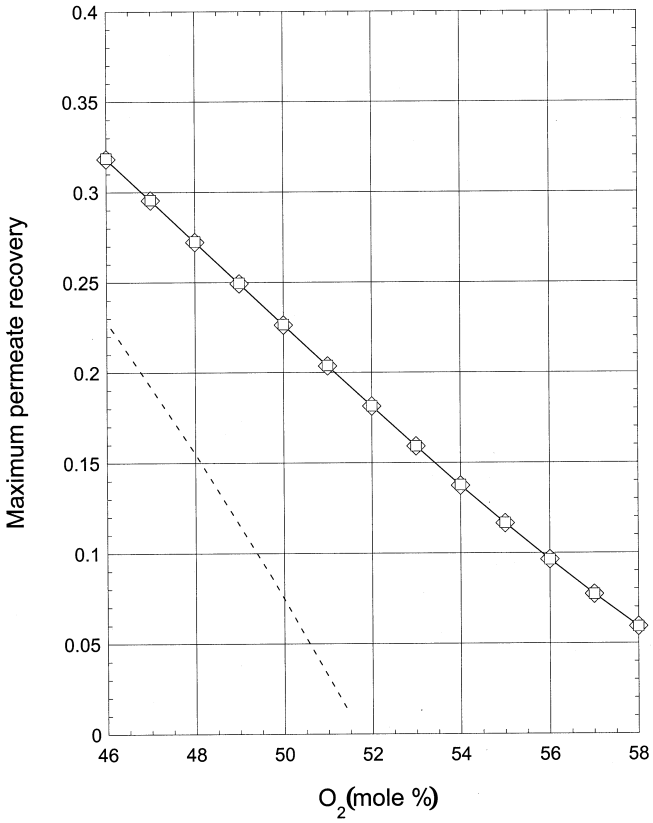

Figure 7. Variation of maximum permeate recovery with regard to O_2 purity: ◇ External two-stage; □ ISP; - - Single stage. The solid line provides a guide for interpreting the external two-stage and ISP results.

MARCEL DEKKER, INC.
270 Madison Avenue, New York, New York 10016

gle countercurrent stage to provide a baseline. Surprisingly, the external two-stage design performs as well as the ISP design.

Both the external two-stage and ISP designs outperformed a single-stage design over the permeate purity range shown. The superior recovery was most pronounced at higher purities. For example, at an oxygen mole fraction of 0.5, the external two-stage and ISP designs provided a permeate recovery almost 3 times greater than that of a single stage.

The values for the pressure of the intermediate-pressure permeate and area ratio, *Ar*, required to maximize permeate recovery for the external two-stage and ISP designs are presented in Figs. 8 and 9. Figure 8 indicates that the optimal pressures for both designs are almost identical. The optimal value decreased

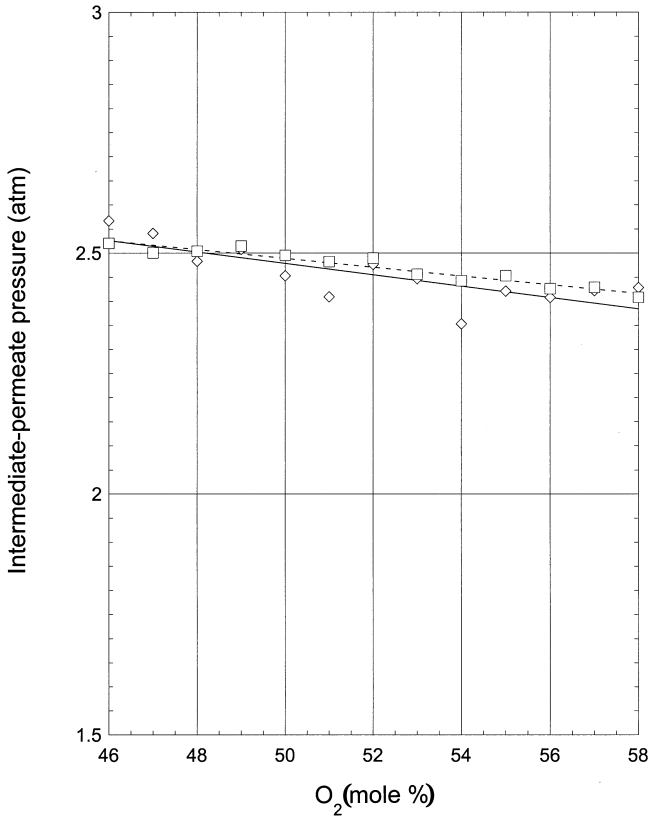

Figure 8. Optimal pressure values for the intermediate-pressure permeate: ◇ External two-stage; □ ISP. The solid and dashed lines provide guides for interpreting the external two-stage and ISP results, respectively.

Marcel Dekker, Inc.
270 Madison Avenue, New York, New York 10016

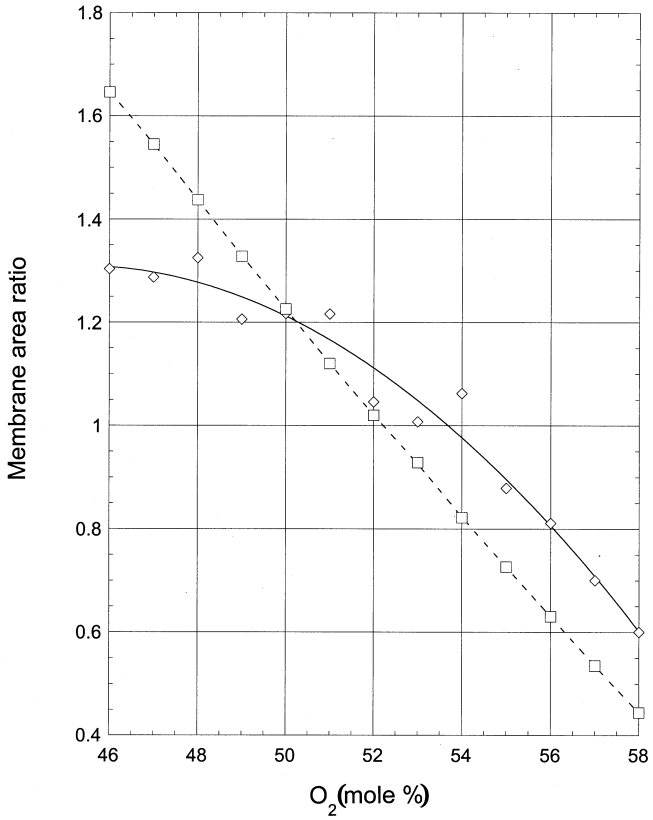

Figure 9. Optimal values of membrane area ratio *Ar*: ◇ External two-stage; □ ISP. The solid and dashed lines provide guides for interpreting the external two-stage and ISP results, respectively.

slightly from 2.6 to 2.4 atm as the oxygen mole fraction increased from 0.46 to 0.58.

Figure 9 indicates that the *Ar* ratio decreased as purity increased. At lower purities, the ISP design required a larger area ratio but the opposite is true at higher purities.

The total, dimensionless membrane area required to maximize permeate recovery is shown in Fig. 10. Both the external two-stage and ISP designs required significantly more membrane area than did a single-stage design; the ISP design requires slightly more area than the external two-stage design. For example, the area required to produce a permeate with $y_L = 0.5$ for the ISP design was approximately 20 times greater than that required for a conventional single-stage system

MARCEL DEKKER, INC.
270 Madison Avenue, New York, New York 10016

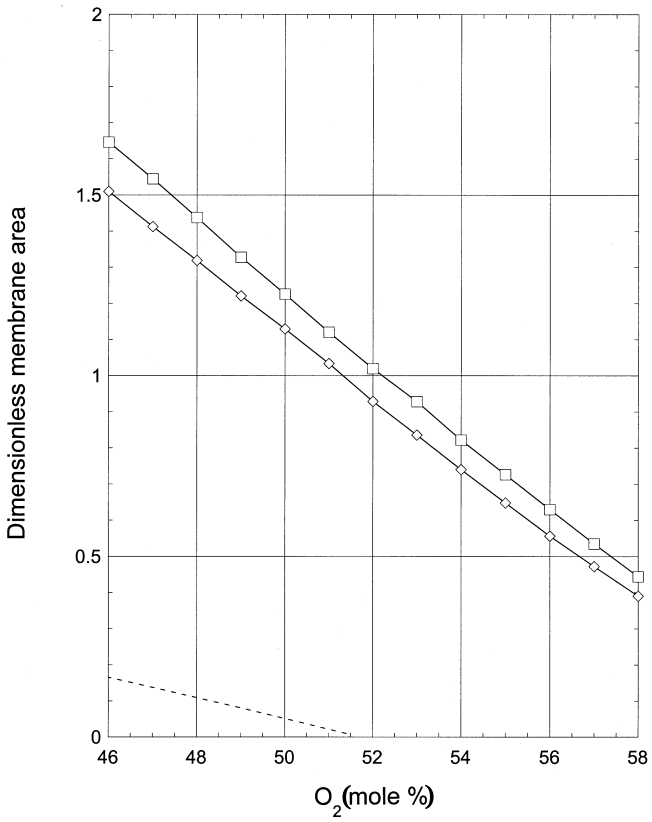

Figure 10. Variation of dimensionless membrane area with O_2 purity: ◇ External two-stage; □ ISP; - - Single stage. The solid lines provide guides for interpreting the external two-stage and ISP results.

and was 8.5% larger than that needed for an external two-stage design. Clearly, the increase in recovery achievable with an ISP or external two-stage design comes at the cost of increased area.

The optimal *Ar* for the external two-stage and ISP varied with product purity. However, the production of systems with turndown capabilities is problematic. Although the patent literature describes designs with such capability, one would prefer to manufacture systems with a fixed area.

To assess the effect of fixing *Ar* on performance, *Ar* was fixed at 1.0, a value in the middle of the optimum range for the external two-stage design, and values of γ_{IH} that maximize recovery were determined using the optimization procedure described previously. The results are shown in Fig. 11. It is interesting that the

maximum recovery achievable with fixed *Ar* is nearly identical to that found with variable *Ar* for the external two-stage design. The required dimensionless membrane area for fixed *Ar* is presented in Fig. 12. The required area was also nearly identical for the external two-stage system in which *Ar* was set at 1 or was variable. For example, at an oxygen mole fraction of 0.5, both the maximum recovery and required area with variable *Ar* differ by less than 1% from the optimal value for fixed $Ar = 1$. This suggests that one can fix *Ar* without significantly affecting the maximum recovery achievable. Researchers in a similar study of ISP designs had reached the same conclusion (16), and the results of those studies are shown in Figs. 11 and 12 for comparison.

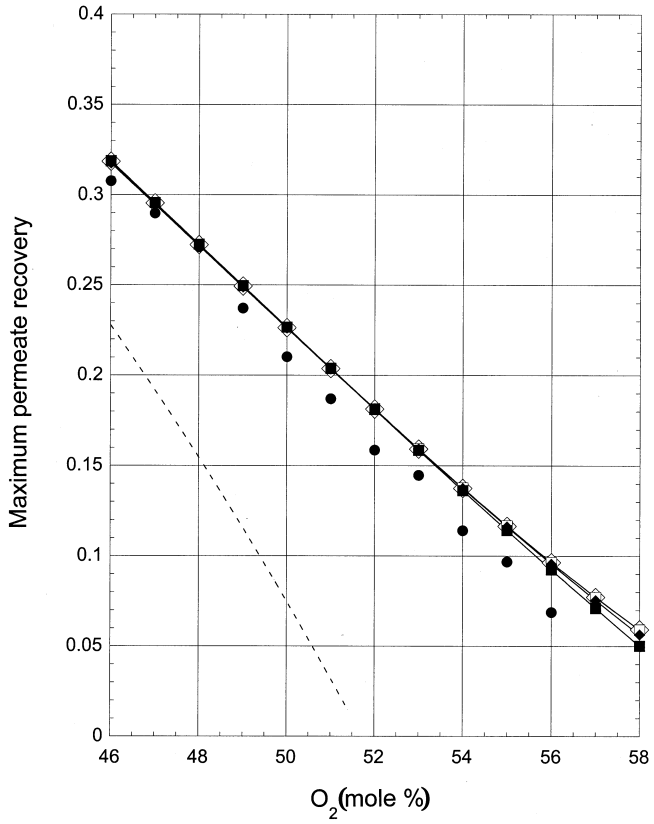

Figure 11. The effect of fixing $Ar = 1.0$ on maximum permeate recovery: ◇ Theory (external two-stage, variable *Ar*); □ Theory (ISP, variable *Ar*); ◆ Theory (external two-stage, $Ar = 1.0$); ■ Theory (ISP, $Ar = 1.0$); ● Experiment (external two-stage, $Ar = 1.0$); - - Theory (single stage). The solid lines provide guides for interpreting the external two-stage and ISP results.

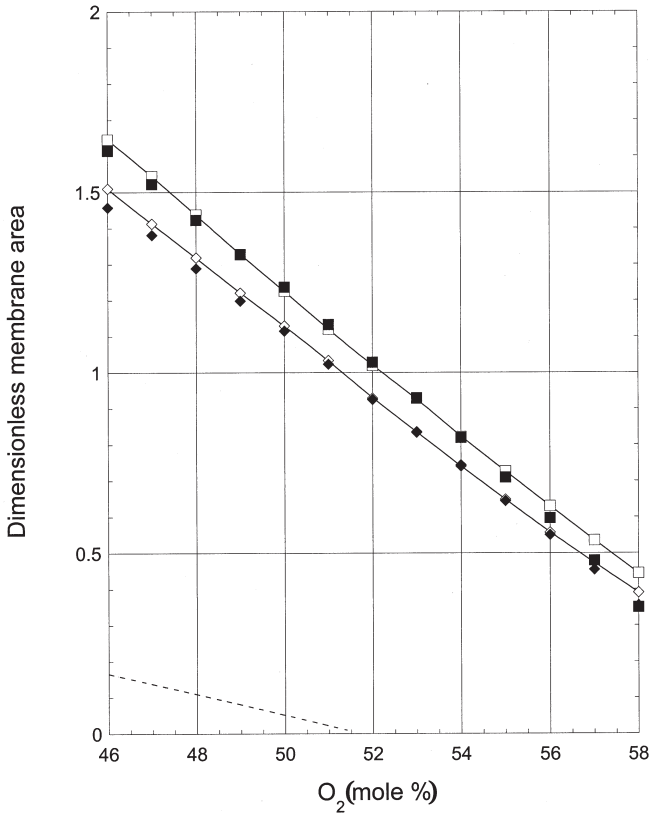

Figure 12. The effect of fixing $Ar = 1.0$ on membrane area: ◇ Theory (external two-stage, variable Ar); □ Theory (ISP, variable Ar); ◆ External two-stage ($Ar = 1.0$); ■ ISP ($Ar = 1.0$); - - Single stage. The solid lines provide guides for interpreting the external two-stage and ISP results.

The optimal value for the intermediate pressure at $Ar = 1.0$ is illustrated in Fig. 13. As in Figs. 11 and 12, theoretical predictions for both the variable and fixed Ar cases are shown. The optimal values for both designs decreased quickly as the permeate purity increased. The values for the external two-stage design were ~0.17 atm greater than those for the ISP design. The optimal pressures for variable Ar lie in the middle of the range found for fixed Ar. In addition, the optimal pressure decreased much faster for fixed Ar than for variable Ar as the purity increased.

Experiments were conducted to confirm the performance predictions for the fixed *Ar* case. The results are shown in Figs. 11 and 13. Figure 13 indicates good agreement between the theoretical and experimental values for the intermediate pressure that maximizes recovery. The experimental recovery, shown in Fig. 11, was slightly lower than the theoretical prediction over the permeate recovery range studied, and as the permeate purity increased, the difference between experiment and theory increased. We attribute these small differences to a combination of fiber property variation and poor shell-flow distribution, which have been shown to be detrimental to performance (19–21).

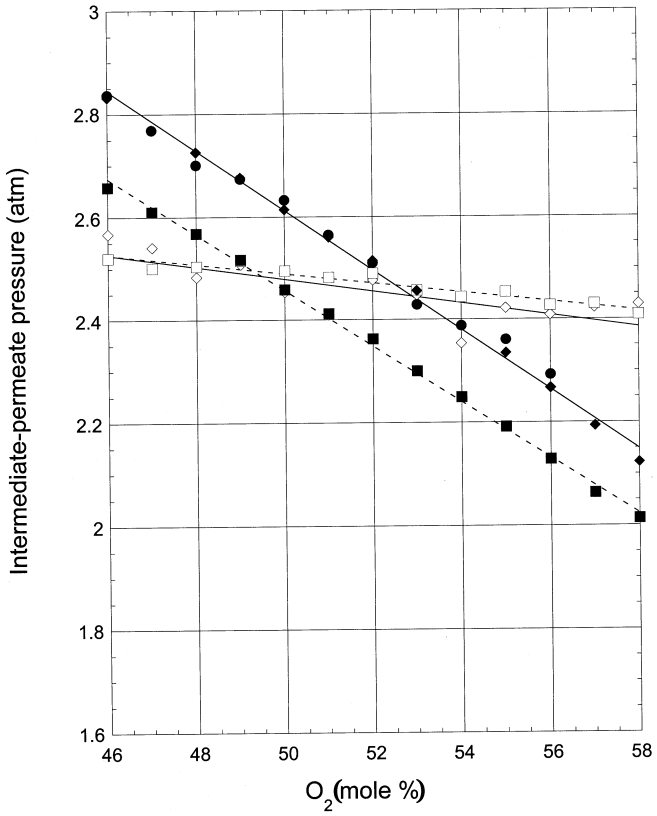

Figure 13. The effect of fixing $Ar = 1.0$ on the optimal pressure values of the intermediate-pressure permeate: ◇ Theory (external two-stage, variable *Ar*); □ Theory (ISP, variable *Ar*); ◆ Theory (external two-stage, $Ar = 1.0$); ■ Theory (ISP, $Ar = 1.0$); ● Experiment (external two-stage, $Ar = 1.0$). The solid and dashed lines provide a guide for interpreting the external two-stage and ISP results, respectively.

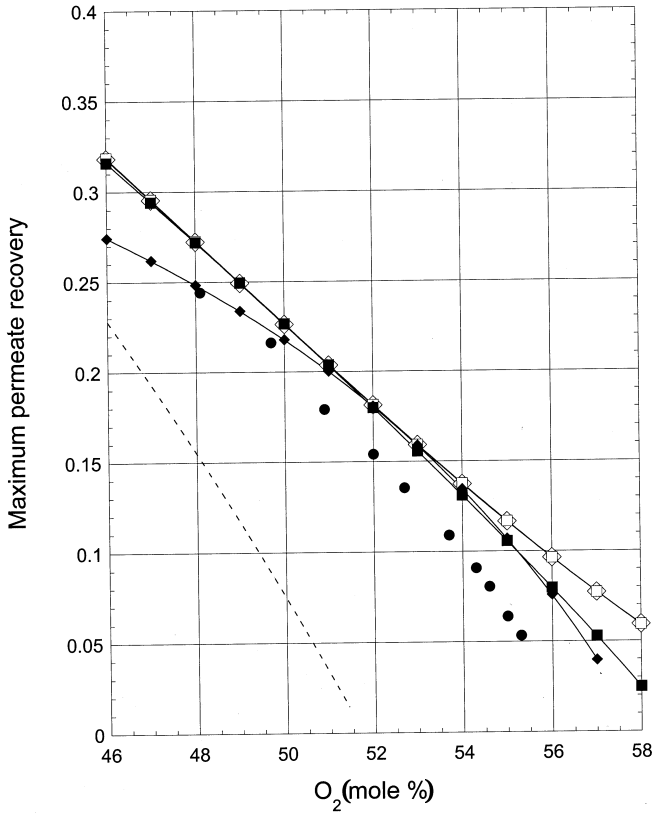

Figure 14. The effect of fixing $Ar = 1.0$ and $\gamma_{IH} = 0.365$ on permeate recovery: ◇ Theory (external two-stage, variable Ar and γ_{IH}); □ Theory (ISP, variable Ar and γ_{IH}); ◆ Theory (external two-stage, $Ar = 1.0$ and $\gamma_{IH} = 0.365$); ■ Theory (ISP, $Ar = 1.0$ and $\gamma_{IH} = 0.365$); ● Experiment (external two-stage, $Ar = 1.0$ and $\gamma_{IH} = 0.365$); - - Theory (single stage). The solid lines provide guides for interpreting the external two-stage and IS results.

Figures 14 and 15 illustrate how performance changes when both Ar ($Ar = 1.0$) and γ_{IH} ($\gamma_{IH} = 0.365$) are fixed; these values lie in the middle of the range of values that gave optimum performance. For comparison purposes, theoretical predictions for the variable Ar and γ_{IH} case are also shown. The reduction in recovery for the external two-stage design at high and low purity is more pronounced than for the case in which only Ar is fixed. For example, when Ar and γ_{IH} are fixed, the recovery for $y_L = 0.46$ dropped from 0.32 to 0.27 and the recovery for $y_L = 0.57$ dropped from 0.08 to 0.05. The required dimensionless area is higher at

MARCEL DEKKER, INC.
270 Madison Avenue, New York, New York 10016

low permeate purity while it is lower at high purity. The performance (permeate recovery) of the ISP design for fixed Ar and γ_{IH} did not change significantly from that of variable Ar and γ_{IH} except at high permeate purity where the recovery is lower. As for the external two-stage design, the required area is higher at low purity and lower at high purity, and the results indicate that the ability to vary γ_{IH} is critical to optimize performance for fixed Ar.

Experiments were also conducted to confirm the performance predictions for fixed Ar ($Ar = 1.0$) and γ_{IH} ($\gamma_{IH} = 0.365$). The experimental results are presented in Fig. 14. The agreement between theory and experiment was comparable to that for the fixed Ar, variable γ_{IH} case.

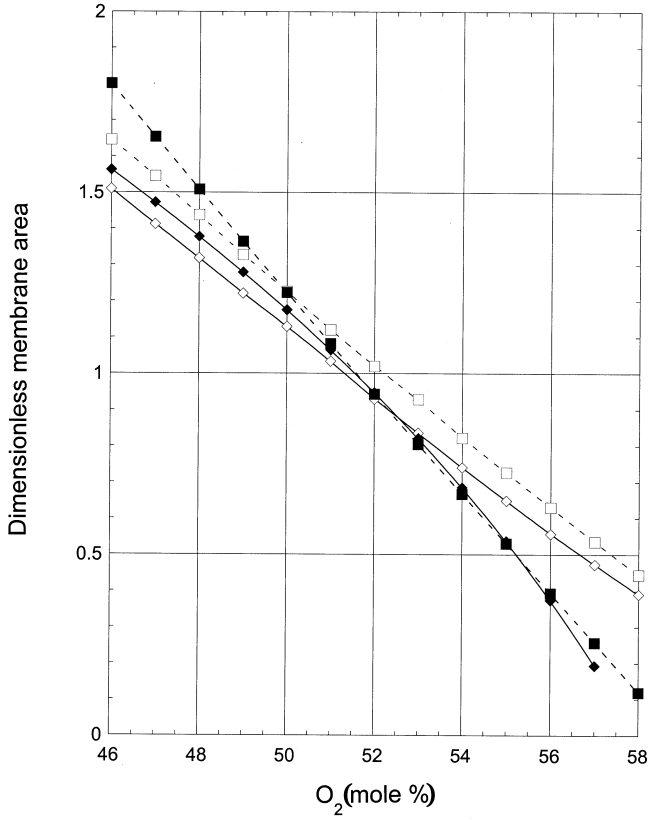

Figure 15. The effect of fixing $Ar = 1.0$ and $\gamma_{IH} = 0.365$ on membrane area: ◇ Theory (external two-stage, variable Ar and γ_{IH}); □ Theory (ISP, variable Ar and γ_{IH}); ◆ Theory (external two-stage, $Ar = 1.0$ and $\gamma_{IH} = 0.365$); ■ Theory (ISP, $Ar = 1.0$ and $\gamma_{IH} = 0.365$). The solid and dashed lines provide guides for interpreting the external two-stage and ISP results, respectively.

CONCLUSIONS

We present an experimental and theoretical study of the co-counter ISP design and a comparable external two-stage design. The co-counter ISP provides the highest permeate recovery of the ISP designs discussed in the literature while the external two-stage design represents a less complex alternative.

For this study, values for the design and operational parameters Ar and γ_{IH} were selected to maximize the recovery of an oxygen-enriched permeate from air. Theoretically, little difference exists between the two optimized designs. The maximum recovery and membrane area requirements for the two designs are nearly identical; the ISP yields slightly higher recovery but requires more area. In addition, the values of Ar and γ_{IH} that optimize performance are similar. Both designs provide higher permeate recovery than a single stage but at the cost of a significant increase in required membrane area.

Experimental measurements for the external two-stage system with $Ar = 1$ are in good agreement with theory. Experimental values for permeate recovery and optimal γ_{IH} agree with predictions. Moreover, the results demonstrate that fixing Ar at a 'near' optimal value does not change performance dramatically. These results suggest that the external two-stage design can yield identical performance to the best ISP. Therefore, the use of an external two-stage system should provide greater manufacturing flexibility (one can produce single-stage or two-stage systems without having to manufacture 2 different fiber bundles) at lower costs. In addition, optimization studies of module cascades need not include ISP designs as a stage option because external two-stage designs provide comparable performance.

NOMENCLATURE

A	membrane area, cm^2
Ar	the ratio of the area available for intermediate to low-pressure permeation to that available for high- to intermediate-pressure permeation
F	feed flow rate, mol/s
J	dimensionless gas-permeation rate
l	effective membrane thickness, cm
N^h	dimensionless mass-transfer coefficient
p	pressure, atm
P	intrinsic slow-gas permeability, cm^3(STP) cm/cm^2s cm Hg
R	retentate flow rate, mol/s
x	fast-gas mole fraction in retentate
y	fast-gas mole fraction in permeate
Z	dimensionless flow-path length

MARCEL DEKKER, INC.
270 Madison Avenue, New York, New York 10016

Greek Letters

α	permselectivity
γ	pressure ratio
θ	ratio of flow rate to feed flow rate

Subscript

H	high-pressure feed
HI	high-pressure feed to intermediate-pressure permeate
I	intermediate-pressure permeate
IH	intermediate-pressure permeate to high-pressure permeate
IL	intermediate-pressure permeate to low-pressure permeate
L	low-pressure permeate
LI	low-pressure permeate to intermediate-pressure permeate
1	first stage
2	second stage

Superscript

A	fast gas
B	slow gas

ACKNOWLEDGMENT

The authors acknowledge partial support of this work by the National Science Foundation through grant CTS-9408414.

REFERENCES

1. Lipscomb, G.G. Design of Hollow Fiber Contactors for Membrane Gas Separations. *The 1996 Membrane Technology Review;* Business Communications Co: Norwalk, CT, 1996; 23–102.
2. McCandless, F.P. A Comparison of Some Recycle Permeators for Gas Separations. J. Membr. Sci. **1985,** *24* (1), 15–28.

3. Majumdar, S.; Heit, L.B.; Sengupta, A.; Sirkar, K.K. An Experimental Investigation of Oxygen Enrichment in a Silicone Capillary Permeator with Permeate Recycle. Ind. Eng. Chem. Res. **1987,** *26* (7), 1434–1441.
4. Naylor, R.W.; Backer, P.O. Enrichment Calculations in Gaseous Diffusion: Large Separation Factor. AIChE J. **1955,** *1* (1), 95–99.
5. Hwang, S.T.; Kammermeyer, K. Operating Lines in Cascade Separation of Binary Mixtures. Can. J. Chem. Eng. **1965,** *43* (1), 36–39.
6. Pan, C.Y.; Habgood, H.W. Gas Separation by Permeation. Part I: Calculation Methods and Parametric Analysis. Can. J. Chem. Eng. **1978,** *56* (4), 197–209 .
7. Pfefferle, W.C. Diffusion Purification of Gases. US Patent 3,144,313, 1964.
8. Hwang, S.T.; Thorman, J.M. The Continuous Membrane Column. AIChE J. **1980,** *26* (4), 558–566.
9. Sidhoum, M.; Majumdar, S.; Bhave, R.R.; Sirkar, K.K. Experimental Behavior of Asymmetric CA Membranes and Its Use in Novel Separation Schemes. AIChE Symp. Ser. **1988,** *84* (261), 102–112.
10. Sidhoum, M.; Majumdar, S.; Sirkar, K.K. An Internally Staged Hollow Fiber Permeator for Gas Separation. AIChE J. **1989,** *35* (5), 764–774.
11. Li, K.; Acharya, D.R.; Hughes, R. Simulation of Gas Separation in an Internally Staged Permeator. Trans. Inst. Chem. Eng. **1991,** *69* (1), 35–42.
12. Li, K.; Acharya, D.R.; Hughes, R. Gas Separation in an Internally Staged Permeator: Experimental Results and Theoretical Predictions. J. Membr. Sci. **1993,** *80* (1–3), 147–156.
13. Chen, Y.S.; Li, K.; Teo, W.K. Performance of Co/Counter-Current and Counter/Co-Current Flow Patterns in an Internally Staged Permeator for Gas Separation. Chem. Eng. Res. Des. **1995,** *73* (A5), 567–574.
14. Li, K.; Hughes, R. Internal Staging for Membrane Gas Separation: Comparison with Conventional Membrane Permeators. Chem. Eng. Sci. **1993,** *48* (22), 3795–3803.
15. Li., K.; Wang, D.; Li, D.; Teo, W.K. Internally Staged Permeator Prepared from Annular Hollow Fibers for Gas Separation. AIChE J. **1998,** *44* (4), 849–858.
16. Liu, B.; Wu, X.; Lipscomb, G.G.; Jensvold, J. Novel Internally Staged Permeator Designs Using a Hollow Fiber Fabric. Sep. Sci. Technol. **2000,** *35* (8), 1153–1177.
17. MATLAB.™ The MathWorks Inc: Natick, Mass.
18. Rautenbach, R.; Struck, A.; Melin, T.; Roks, M.F.M. Impact of Operating Pressure on the Permeance of Hollow Fiber Gas Separation Membranes. J. Membr. Sci., **1998,** *146* (2), 217–223.
19. Rautenbach, R.; Struck, A.; Roks, M.F.M. A Variation in Fiber Properties Affects the Performance of Defect-Free Hollow Fiber Membrane Modules for Air Separation. J. Membr. Sci. **1998,** *150* (1), 31–41.

MARCEL DEKKER, INC.
270 Madison Avenue, New York, New York 10016

20. Lemanski, J.; Liu, B.; Lipscomb, G.G. Effect of Fiber Variation on the Performance of Cross-Flow Hollow Fiber Gas Separation Modules. J. Membr. Sci. **1999,** *153* (1), 33–43.
21. Bao, L.; Liu, B.; Lipscomb, G.G. Entry Mass Transfer in Axial Flows Through Randomly Packed Fiber Bundles. AIChE J. **1999,** *45* (11), 2346–2356.

Received May 2000
Revised November 2000

MARCEL DEKKER, INC.
270 Madison Avenue, New York, New York 10016

Request Permission or Order Reprints Instantly!